Catalysis Today 382 (2021) 130–141

Contents lists available at ScienceDirect

Catalysis Today

journal homepage: www.elsevier.com/locate/cattod

Modifying the catalytic properties of hydrotreating NiMo–S phases by changing the electrodonor capacity of the support

Carlos López-Cruz [a,b], Javier Guzman [c], Guang Cao [c], Cristina Martínez [a,*], Avelino Corma [a,*]

[a] Instituto de Tecnología Química, Universitat Politècnica de València-Consejo Superior de Investigaciones Científicas, Avenida de los Naranjos s/n, 46022 Valencia, Spain
[b] Technical Department of International Flavors & Fragrances (IFF), Av. Felipe Klein 2, 12580 Benicarló, Spain
[c] ExxonMobil Research and Engineering Co. Annandale, 08801 NJ, United States

ARTICLE INFO

Keywords:
Hydrotreating catalyst
MgAl layered double hydroxides
MgO
Al_2O_3
Electronic support effects
NiMo–S phase

ABSTRACT

The hydrogenation activity and physico-chemical characterization of a series of NiMo catalyst supported on materials with different acid-base properties (Al_2O_3, layered double hydroxides-derived MgAl oxides and MgO) have been investigated. The results show a clear correlation between the electrodonor capacity of the support, the negative charge density of the supported NiMo oxides and the intrinsic hydrogenation rate of the sulfided phase. Spectroscopic characterization ruled out any possible contribution derived from differences in the $NiMoS_2$ stack or slab size distributions, as determined by high-resolution transmission electron microscopy. The experimental results obtained suggest the occurrence of an electron transfer phenomena from the support to the supported $NiMoS_2$ slabs, being this effect stronger for supports with higher electrodonor capacity.

This work presents a specific electronic support effect that goes beyond the classical dispersing and stabilizing role.

1. Introduction

Transition metal (TM) based catalysts are a unique class able to perform hydrogenation and heteroatom removal reactions in the presence of sulfur. Continuous research and development has allowed improving their catalytic performance in order to meet the continuously increasing environmental regulations on S and N content of fuels. Metal promotion by Ni or Co has been one of the most important findings that allowed bringing the TMs catalysts to a higher level of efficiency [1,2]. The cause behind the Ni or Co promotion effect is still nowadays a matter of controversy. The most commonly accepted explanation proposed that the promotional effect of Ni (or Co) on the activity of MoS_2 arises from the interaction between the 4d electrons of Mo atoms and the 3d electrons of the second metal [3–7], Ni or Co. This interaction would occur through an electronic transfer between the promoting metals and the MoS_2. As a result the 4d orbitals of Mo atoms would be filled with additional electrons favoring the formation of vacancies on the MoS_2, where aromatic or sulfur containing compounds would be adsorbed and activated.

Since the discovery of TMs catalysts, different models have been proposed to understand, explain and correlate their catalytic performance on basis of their physico-chemical properties. First models such as the "monolayer" [8], the "pseudointercalation" [9,10] or the "contact synergy" model [11] are nowadays already discarded. Yet, they set up the basis for the development of more complex models such as the RIM-EDGE model proposed by Chianelli et al. in the 80 s [12]. This model is one of the most commonly accepted and nowadays it is still employed to interpret catalytic results [13–15]. According to the authors, active sites (RIM sites) capable of catalyzing hydrodesulfuration (HDS) as well as hydrogenation (HYD) reactions are located exclusively at the edge and corner positions of single MoS_2 slabs. Upon stacking, MoS_2 slabs located in interlaminar positions catalyze uniquely hydrodesulfurization reactions by the direct desulfurization path (DDS). The slabs with one of their MoS_2 basal plane exposed to reactant molecules would hold the so-called RIM sites capable of hydrogenating reactions.

Later on, the group of Topsoe proposed the "edge decoration" model based on the first experimental evidence of a specific CoMo sulfided phase characterized by Emission Mossbauer spectroscopy [16–18]. HR-TEM measurements allowed confirming the presence of Co decorating the MoS_2 edges [19]. In addition, a correlation between HDS activity and the number of these edge CoMo-S sites was demonstrated [17]. Additional studies by this research group allowed differentiating

* Corresponding authors.
E-mail addresses: cmsanche@itq.upv.es (C. Martínez), acorma@itq.upv.es (A. Corma).

https://doi.org/10.1016/j.cattod.2021.08.002
Received 8 February 2021; Received in revised form 9 July 2021; Accepted 4 August 2021
Available online 8 August 2021

between two different Co(or Ni)Mo sites, so called type I and type II, found in monolayered MoS_2 and multilayered MoS_2 structures, respectively [20]. Each type of sites exhibited different HDS activity, which the authors postulated to be related to undefined structural or electronic effects induced by the support. The actual structure of a single MoS_2 layer was showed by a series of impressive and inspiring STM (scanning tunnel microscopy) images of MoS_2 supported on a gold grid [21] and later also on graphite or TiO_2 [22,23].

Despite the significant advances of the last years, the complete picture of TMs catalysts remains nowadays still unclear. For instance, there is no agreement in the literature about the most convenient NiMo-S phase (I or II) in terms of catalytic activity. The type I phase is less active but better dispersed than type II. Therefore, a priori, it cannot be stated whether phase I or II will achieve the optimum catalytic activity on a given support. Moreover, CoMo and NiMo hydrotreatment catalysts have been described as dynamic systems that interact and adapt themselves to the evolving reaction environment [24]. The active sites will be, therefore, in continuous evolution, and will interact with the reactant molecules according to their specific state in each moment. On the other hand, sulfided phases are normally described as type I or type II depending on the stacking degree observed by HR-TEM, and density functional theory (DFT) studies have shown the importance of active site accessibility in multilayer unsupported $NiMoS_2$ when converting bulky substrates such as 4,6-DMDBT [25].

In contrast with this general assumption, Eijsbouts et al. [26] observed that a typical type II (NiMo) commercial catalyst sulfided in the liquid phase did not show the typically stacked morphology reported for these MoS_2 phase. Therefore, the authors proposed that the stacked structure generally ascribed to the type II Ni(or Co)Mo–S phase may not be a specific feature but a circumstantial one due to the low interaction of MoS_2 with the support in combination with a severe sulfidation procedure.

As commonly agreed in the literature, the catalytic activity of TM catalysts results from a complex interrelation between different effects related to the support (surface area, metal-support interaction), the metal promotion (nature of the metal promoters, efficiency of edge decoration vs phase segregation), the nature of the MoS_2 phase (type I vs II, slab size, stacking…) and, of course, the preparation and activation procedures. Many different materials (TiO_2, Al_2O_3, SiO_2, $SiO_2Al_2O_3$, MgO, mixed oxides, activated carbon…) and metal promoters (Ni, Co, Cu, Fe,….) have been tested for developing (NiCo promoted) Mo/W hydrotreating catalyst [27–32]. The results obtained cannot always be explained merely on the basis of metal promotion, type and/or dispersion of the metal sulfided phase (I vs II) formed. This suggests that there are additional effects playing an important role in the catalytic performance of TMs catalysts. Therefore, although initially the support of TMs catalysts was considered as a dispersing and stabilizing agent of the sulfided phase, unexplained results are often (unsatisfactory) ascribed to undefined support effects on the metal-sulfided active phase [33].

MgO [34–39] and Al_2O_3MgO mixed oxides [40–44] have been investigated as alternative to the traditional Al_2O_3 support for CoMo- or NiMo-based HDS catalysts. In general, it is reported that the basicity of these materials increases the dispersion and stabilization of the NiMo-S phase and limits the formation of coke during the reaction. Yet, it has been observed on NiMo catalyst that the strong metal support interaction leads to the formation of NiO–MgO and NiO–Al_2O_3 solid solutions which reduces the promoting effect of Ni [40,42]. Rana et al. [41] investigated the use of CoMo/MgOAl_2O_3 catalysts for (mild) hydrotreating of heavy feeds with promising results. The strong metal support interaction was partially avoided by using different chelating agents during the metal incorporation procedure. The authors reported better catalytic performance for catalysts with higher MgO content. This effect has been attributed to an increase of pore diameter of the support and to a decreased coking tendency of the catalysts due to the presence of MgO in the support material. Yet, remarkable differences regarding the dispersion of the sulfided phase (stacking, slab length) were also observed. Therefore, additional effects playing a role in the catalytic performance of these catalysts could not be discarded.

The potential influence of basic supports such as MgO or MgOAl_2O_3, has only been discussed in terms of dispersion of the NiMo–S phase or loss of metal promotion due to the formation of solid solutions. However, considering that the promotional effect of Ni (or Co) on the MoS_2 slabs is based, as mentioned before, on an electron transfer mechanism, one may consider that the electrodonor capacity of basic materials may also play a role in the catalytic performance of the supported NiMo-S phase.

With the purpose of getting some insights over possible support effects (beyond the dispersing one) on the NiMo–S phase, the physicochemical properties and hydrogenation activity of a series of catalysts supported on a series of materials of increasing basicity (Al_2O_3, MgAl-LDHs and MgO) have been investigated.

2. Experimental

2.1. Synthesis of layered MgAl hydroxides

MgAl LDH have been prepared by a co-precipitation method as described by Climent et al. [45]. The nitrates of Al and Mg were dissolved in milliQ-water. The resulting mixture was then added to an alkaline solution containing anhydrous sodium carbonate and sodium hydroxide using a syringe pump at a speed of 1 ml min^{-1} at room temperature. After aging for 18 h at room temperature, the solution was filtered and washed until pH of the washing waters was 7.0. The obtained (wet) solid was dried in an oven at 60 ºC overnight.

Following the procedure described above, three different MgAl LDH samples have been prepared with $Al^{3+}/(Al^{3+}+Mg^{2+})$ ratios of 0.20, 0.25 and 0.33. For the sake of simplicity the samples have been labeled as MA20, MA25 and MA33, respectively.

2.2. Catalysts preparation

NiMo/MA*X* (*X* =20, 25 or 33, see former section) catalysts have been prepared by impregnation of the non calcined LDH materials following the well-known 2-step sequential incipient wetness impregnation procedure. Ammonium heptamolybdate (AHM) and nickel nitrate (NN) in aqueous solutions were used as Mo and Ni source.

After impregnation with AHM, the sample was aged in a desiccator overnight and dried at 100 °C overnight. The resulting solid was impregnated with NN, and calcined at 500 °C for six hours. The samples have been labeled as *x*NiyMo/LDH, where *x* and *y* indicate the content of the Ni and Mo oxides, respectively (as wt%), and LDH is the corresponding LDH precursor.

Alumina- and MgO-based catalysts have been prepared following the same methodology and labeled as *x*NiyMo/Al_2O_3 and *x*NiyMo/MgO, respectively.

2.3. Characterization techniques

Specific surface areas were determined in a Micromeritics ASAP 2000 equipment by means of nitrogen adsorption at 77 K and applying the BET-method. Prior to the adsorption measurements, the samples were degassed at 450 °C for 24 h.

The chemical composition of the catalysts was determined by means of a 715-ES inductively coupled plasma (ICP) Optical Emission spectrometer, after dissolution of the solids in a HNO_3/HF solution.

The structure of the solids was confirmed by powder X-ray diffraction (XRD) using a Philips X′Pert diffractometer equipped with a graphite monochromator, operating at 40 kV and 45 mA and using nickel-filtered Cu Kα radiation (λ = 0.1542).

HR-TEM micrographs of the sulfided catalyst were recorded in a FEI-TECNAI G2 microscope system with an operating voltage of 200 kV. Catalysts were sulfided ex-situ prior to the TEM measurement. Although

exposition to air could not be completely avoided (loading of samples into the HR-TEM cell), it was reduced as much as possible by cooling down the sulfided samples to room temperature (in H_2S atmosphere) and transferring them into the dispersing media (methanol) under inert atmosphere prior to HR-TEM measurement.

X-ray photoelectron spectroscopy (XPS) measurements were performed on a SPECS spectrometer with a MCD-9 detector and using a non monochromatic AlKa (1486.6 eV) X-ray source. Spectra were recorded using analyzer pass energy of 50 V, an X-ray power of 200 W and under an operating pressure of 10–9 mbar. Spectra treatment has been performed using the CASA software. Binding energies (BE) were referenced to C1s at 284.5 eV.

2.4. Reaction tests

2.4.1. Knoevenagel condensation

Knoevenagel condensation has been used as a test reaction for measuring the basicity of the support materials. The tests have been carried out employing benzaldehyde (10 mmol, BZ), and ethyl cyanoacetate (10 mmol, ECA). The reactant mixture was magnetically stirred under nitrogen atmosphere, while heating up to the reaction temperature (60 °C) in an in house built batch reaction system. Then, 4% (wt/wt) of hydrotalcite catalysts was added and the reaction started. Samples were taken periodically, and the evolution of the reaction was followed by taking samples at different reaction times and analyzing the products by gas chromatography. The basicity has been evaluated as the initial reaction rate, obtained from the conversion vs reaction time curve for conversion levels below 15%.

2.4.2. Hydrogenation of 1-methylnaphthalene

Hydrotreating tests with a model feed were performed in a fixed-bed stainless-steel tubular reactor having a 1/4 in. i.d and 20 cm length. The model feed was composed of 10 wt% of 1-methylnaphthalene (1-MN), 2 wt% of dimethyldisulfide (DMDS), 500 ppm of dibenzothiophene (DBT) and normal heptane (n-C7) 87.95%. The additive DMDS was aimed to decomposes quickly to give H_2S, allowing in this way a simulation of the experimental conditions with industrial HDS feeds (2–3 wt% H_2S) and preventing the reduction of the metal sulfides with TOS. The reactor was charged with 0.5 g (otherwise indicated) of catalyst with a particle size of 0.2 to 0.4 mm diameter and diluted with SiC up to a 3:1 (SiC to cat) volume ratio. Gaseous reactants (H_2, Ar and H_2S) were fed into the system by means of mass flow meters via the vaporizer. The liquid model mixture was fed by a HPLC pump to the vaporizer. The design of the vaporizer and its operating temperature (300 °C) were critical in establishing a steady (non pulsing) flow of reactants to the reactor.

Prior to the catalytic test, unless otherwise indicated, the catalyst was pre-sulfided in situ at 5 bar and 400 °C in a H_2S/H_2 (10 vol% H_2S, 200 ml/min) stream for 4 h. The reaction conditions were 30 bar, 350 °C, LHSV of 0.125 h^{-1} and a H_2/feed ratio of 1000 Nm^3/m^3. During reaction, the effluent stream was analyzed on line at intervals of 30 min in a Varian 3400 equipped with a Factor Four™ column and thermal conductivity and flame ionization detectors (TCD and FID, respectively). Argon was employed as internal reference allowing an accurate quantification of the amount and distribution of reaction products. Identification of reaction products was performed by GC employing a HP6890N with a HP5MS column (30 m) coupled with a HP5973 mass selective detector.

3. Results and discussion

3.1. Catalyst characterization

A series of NiMo catalysts were prepared employing as support a variety of materials within a wide range of acid-base properties: two different types of Al_2O_3, three MgAl LDH's with different Mg/Al ratio, and MgO. Ni and Mo were incorporated on each of the support materials following conventional aqueous impregnation procedure as described in the experimental section. Table 1 shows the different catalyst prepared and their main physico-chemical properties, including metal loadings, Ni/Mo atomic ratios and textural properties of the calcined samples. Despite the much higher BET surface area of the parent TM-free MgO support (see Table 1, values in brackets) after metal incorporation and calcination the specific surface area decreases to values intermediates as compared to the two different aluminas and the LDH's, whose textural propertied are preserved in a larger extend after TM loading.

As can be seen, LDH-based catalysts were loaded with ~ 20 wt% of Mo and maintaining a Ni/Mo atomic ratio of 0.6. Two Al_2O_3-based catalysts (regular γ-Al_2O_3 and high surface area alumina) were also prepared following what is commonly reported in the open literature as the optimum Mo loading and Ni/Mo ratio [2], i.e., $^{3}Ni^{12}Mo/Al_2O_3$, $^{3}Ni^{12}Mo/Al_2O_3$-HS. A third alumina-based catalyst, $^{6}Ni^{20}Mo/Al_2O_3$-HS, has been loaded with similar amounts of Mo and Ni as compared to the LDH-based catalysts. This sample, although not optimized, is very similar in terms of textural properties and metal loading to the catalysts supported on LDH, and has been prepared for comparison purposes. Finally, a MgO-based catalyst, $^{3}Ni^{12}/MgO$, has been prepared mimicking the procedure and the Ni and Mo loadings reported for Al_2O_3.

The basicity of the different support materials was evaluated by means of the Knoevenagel test reaction as described in the experimental section. According to the results, enclosed in Table 1, MgO is the most basic support, followed by the LDH-derived MgAl oxides (MA20 > MA25 > MA33, in good agreement with their Mg content) and the alumina (Al_2O_3-HS > Al_2O_3). After the Mo and Ni incorporation, the basicity of each material decreased noticeably but the trend observed was the same.

The properties of the different catalyst in their sulfided form were investigated by different spectroscopic techniques. Firstly, the NiMo-S phase of the different catalysts was characterized by high resolution transmission electron microscopy (HR-TEM). It is well known that MoS_2 slabs can adopt a flat-wise or edge-on orientation with respect to the support (see Scheme 1). Unfortunately, only the edge planes of the laminar MoS_2 clusters oriented in line with or slightly tilted from the electron beam are visible by HR-TEM. Therefore, strictly speaking, this technique provides uniquely a partial picture of the MoS_2 phase analyzed [46]. The contact of the sulfided samples with air, although kept at minimum, could not be completely avoided. The studies of the detrimental effect of air exposure on MoS_2 slabs have been reported in the literature by Kooyman et al. [47]. According to the authors, samples obtained by gas phase sulfidation (H_2S) do not show significant changes on the morphology and distribution of MoS_2 slab size after air exposure

Table 1
Main physico-chemical characterization of the different NiMo catalyst.

Sample	NiO (wt %)	MoO_3 (wt%)	Ni/Mo (at/at)	BET surface Area (m^2/g)	Pore volume (cc/g)	Support basicity [(a)]
$^{3}Ni^{12}Mo/MgO$	3.4	12.7	0.51	153.8 (594.7)	0.67	1.50
$^{6}Ni^{19}Mo/MA20$	6.4	19.0	0.65	260.7 (263.5)	0.51	1.13
$^{6}Ni^{19}Mo/MA25$	5.3	19.0	0.54	249.3 (259.3)	0.60	0.66
$^{6}Ni^{19}Mo/MA33$	5.2	18.7	0.54	264.7 (270.2)	0.60	0.33
$^{3}Ni^{12}Mo/Al_2O_3$	3.0	12.0	0.49	114.2 (146.1)	0.29	0.17
$^{3}Ni^{12}Mo/Al_2O_3$-HS	3–0	12.2	0.47	239.3 (230.2)	0.51	0.28
$^{6}Ni^{20}Mo/Al_2O_3$-HS	5.2	20.0	0.50	232.7 (230.2)	0.49	0.28

[(a)] Basicity as evaluated by the Knoevenagel test (mol/g/min·10–2)

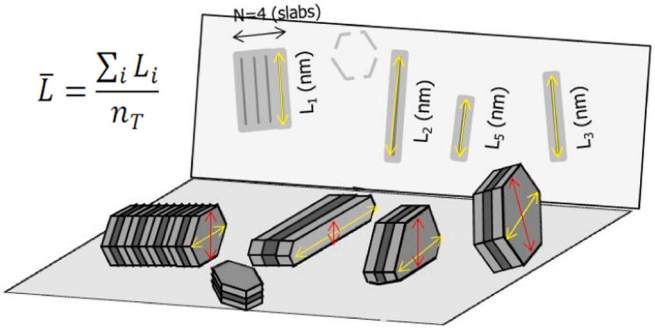

$$\bar{L} = \frac{\sum_i L_i}{n_T}$$

$$Stk = \frac{\sum_i^{Stack} L_i}{\sum_i^{Single\ slab} L_i}$$

$$N = \sum_i \left({}^{P_i}/_{100} \cdot N_i \right)$$

L: Length of a single slab

P_i: Percentace of stacks

Scheme 1. Schematic representation of the HR-TEM picture and the main parameters determined.

(24 h). Therefore, the relatively large (Ni)MoS_2 slab sizes obtained for our series of samples and the short exposure to air allows discarding any significant effect due to reoxidation of $NiMoS_2$ during their loading in the HR-TEM measurement cell. Moreover, and despite the well-known limitations, there are many examples in the literature proving that TEM is, in many cases, a useful technique for describing sulfided TMs phases, providing good correlations with their catalytic activities [13].

Representative HR-TEM pictures of each catalyst are included in Fig. 1. As can be seen there at eyes sight, only the catalyst $^{3}Ni^{12}Mo/MgO$ presents clear differences as compared to the rest. Mainly single, long MoS_2 slabs can be found on the catalyst surface, and (Ni)MoS_2 stacks are hardly seen, in good agreement with previous results on MgO-based catalyst [34]. Al_2O_3- and LDH-based catalysts present single MoS_2 slabs as well as MoS_2 stacks of several slabs. In order to perform a proper comparison between the different samples, the slab and stack size distributions have been obtained for each catalyst based on particle populations of 1000–1200. The results are included in Fig. 2.

As can be seen, MgO-based catalyst presents a relatively wide and left tailored $NiMoS_2$ slab size distribution with a maximum at ca 2.5 nm. Stacking does not take place at a significant extent and most of the $NiMoS_2$ phase is present as single $NiMoS_2$ slabs. Alumina-based catalysts loaded with the same Ni and Mo loadings as MgO show a narrower slab size distribution, especially the $^{3}Ni^{12}Mo/Al_2O_3$-HS catalyst but, besides single slabs, a higher stacking degree is observed for these two samples, intermediate between that of the MgO- and LDH-based catalysts. For metal loadings above the optimal one, $^{6}Ni^{20}Mo/Al_2O_3$-HS shows a significant widening and shifting of the $NiMoS_2$ slab size distributions towards bigger sizes as compared to $^{3}Ni^{12}Mo/Al_2O_3$-HS. Yet, the stacking degree remains similar to that of alumina-based catalyst with lower metal content.

LDH-based catalysts present a $NiMoS_2$ slab size distribution slightly narrowed and shifted toward smaller sizes as compared to $^{3}Ni^{12}Mo/MgO$. The most significant difference among the MgO-based catalyst and the LDH-based ones is the stacking degree of the NiMo–S phase, much higher for the latter ones.

On the basis of the slab size distributions, the average slab size (L), the stacking degree (Stk) and the average size of the stacks (N, the average number of slabs per stack) has been determined (see Scheme 1). As Fig. 2 suggested, alumina-based catalysts presents the smallest average slab size (L) followed by the LDH-based catalyst (all of them showing a similar slab size between 3.3 and 3.6 nm). Catalyst $^{3}Ni^{12}Mo/MgO$ presents the biggest average $NiMoS_2$ slab size of this series of catalysts. MgO- and alumina-based catalysts, in this order, presented the lowest stacking degree. The LDH-based catalysts, despite having similar textural properties as the Al_2O_3-based samples, present a significantly higher stacking degree than the former two, varying from 40% up to 55%.

The results obtained with the series of Al_2O_3-based catalysts show that the surface area and metal loading have an effect on the dispersion of the NiMo–S phase. In addition, the comparison of the former with the LDH and MgO-based catalysts shows that, besides the textural properties, the nature of the support has also a significant impact on the dispersion of the sulfided phase. This indicates that the metal support interaction is different for MgO, LDH or Al_2O_3-based catalysts. Therefore, in order to get insights on this effect and to obtain experimental evidences, some representative samples of this series have been investigated by X-ray Photoelectron Spectroscopy (XPS).

Figs. 3 and 4 show the Ni $2p_{3/2}$ and Mo $3d_{5/2}$ components of the Ni and Mo supported oxides, respectively, for the MgAl(LDH)-, Al_2O_3-, and MgO-based catalysts in their calcined form. Deconvolution of each component has been carried out by means of the CASA software (ver. 2.3.16Dev52) in order to identify the different species contributing to the overall bands observed.

The Ni $2p_{3/2}$ component of LDH-based catalyst is centered at binding energies (BE) of ca 857 eV, as can be seen in Fig. 3. This Ni component has been resolved in two bands attributed to the spin-splitting of Ni $2p_{3/2}$. The broad peak at higher BE values (ca 864–865 eV) corresponds to the envelopes of the corresponding shakeup satellites. The band centered at 855.8–856.2 eV (depending of the sample) can be ascribed to Ni(Al_2O_4), Ni_2O_3, NiO or $NiMoO_4$ [48–50]. According to the literature, the high symmetry of this peak and the shakeup satellite structure at ca 862 eV allows discarding the presence of Ni_2O_3 [49]. On the other hand, the second band at ca 856.7–857 eV (Ni $2p^{3/2}$) can be assigned to $NiAl_2O_4$ [51]. Thus, according to the XPS spectra, NiO, $NiMoO_4$ and $NiAl_2O_4$ are present on the surface of the calcined LDH-based catalysts.

Fig. 3 shows the XPS spectra of the Mo3d component for the different catalysts. Two bands centered at BE of ca 229.3 eV ($Mo3d_{5/2}$) and ca 231 ± 1 eV($Mo3d_{3/2}$) have been assigned. The first band corresponds to isolated MoO_4 species, Mo_4O_{11} [52] or MoOx [52,53], and the later corresponds to $NiMoO_4$ and MoO_3 [48,49].

The XPS spectrum of $NiMo/Al_2O_3$-HS catalyst is included in Fig. 4a and -b for the Ni and Mo component, respectively. $NiMo/Al_2O_3$-HS presents two different contributions to the Ni2p3/2 component. According to the BE values, 856.7 and 857.4 eV, and peak width, these XPS bands can be attributed to NiO and/or $NiMoO_4$ and $NiAl_2O_4$, respectively [48–51]. On the other hand, the Mo 3d component presents a single contribution. The BE value and peak width (232.6 eV and 2.4, respectively) indicates the presence of MoO_3 [48,49].

Finally, the XPS spectra of the NiMo/MgO catalyst are included in Fig. 4. As can be seen, the Ni2p component (Fig. 4c) shows two different contributions. According to the BE values [48], the Ni species can be ascribed to NiO and/or $NiMoO_4$ (855.3 eV) and Ni^0 (852.2 eV). On the other hand, the Mo 3d (Fig. 4d) presents a unique contribution at 232.2 eV which is ascribed to MoO_3 [48,49].

The results of the deconvoluted spectrum are summarized in Table 2. As can be seen, the BE values found for the different Ni and Mo species on the $NiMo/Al_2O_3$-HS catalyst are slightly shifted towards higher values as compared to those of the LDH-based catalysts. On the other hand, catalyst NiMo/MgO presents for the Ni component (NiO and/or $NiMoO_4$), a BE value around − 0.5 eV lower than that of the LDH-derived catalysts.

It is also interesting to notice that for the catalysts containing Al, the

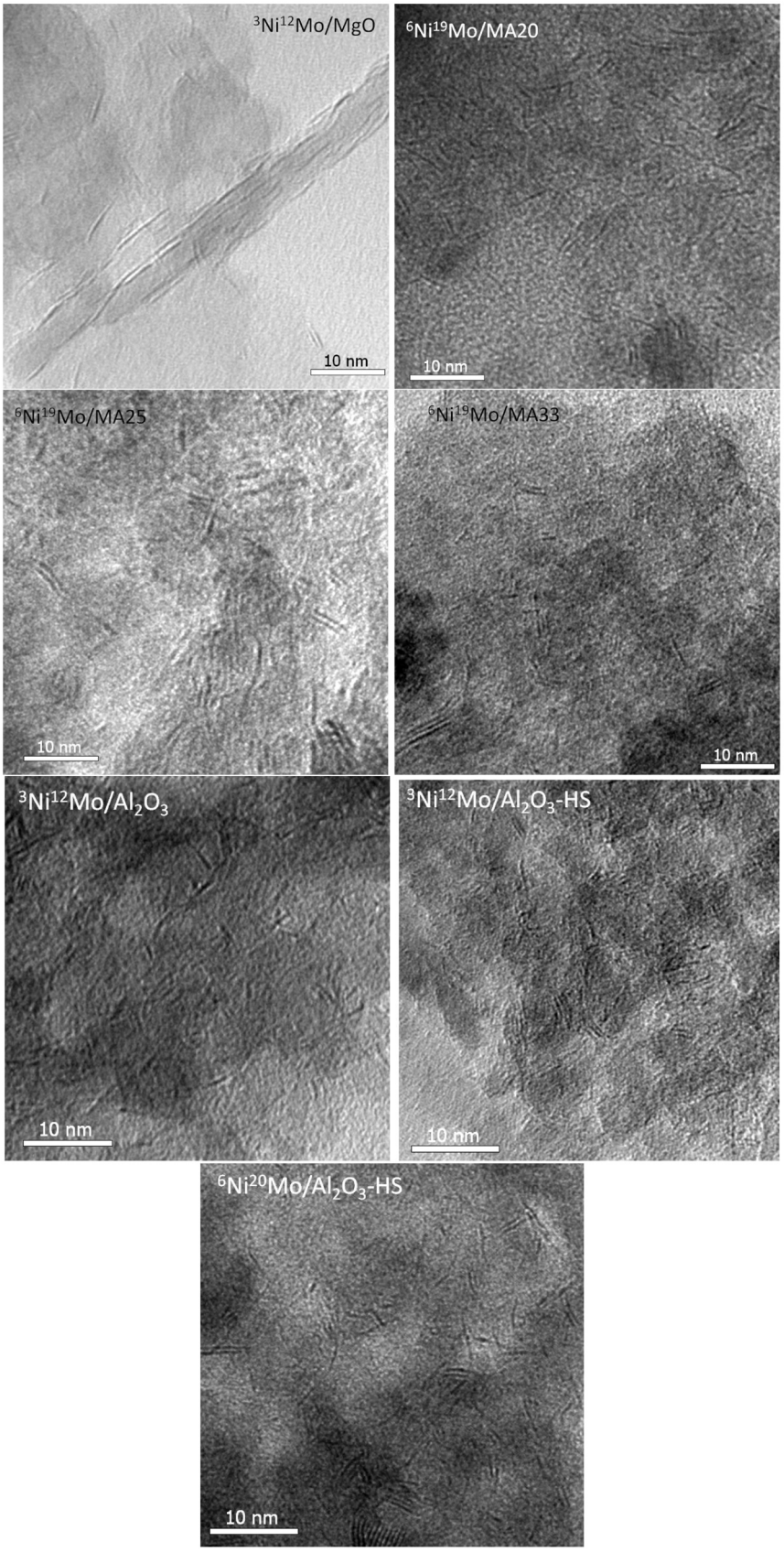

Fig. 1. HR-TEM micrographs of the different NiMo supported catalysts.

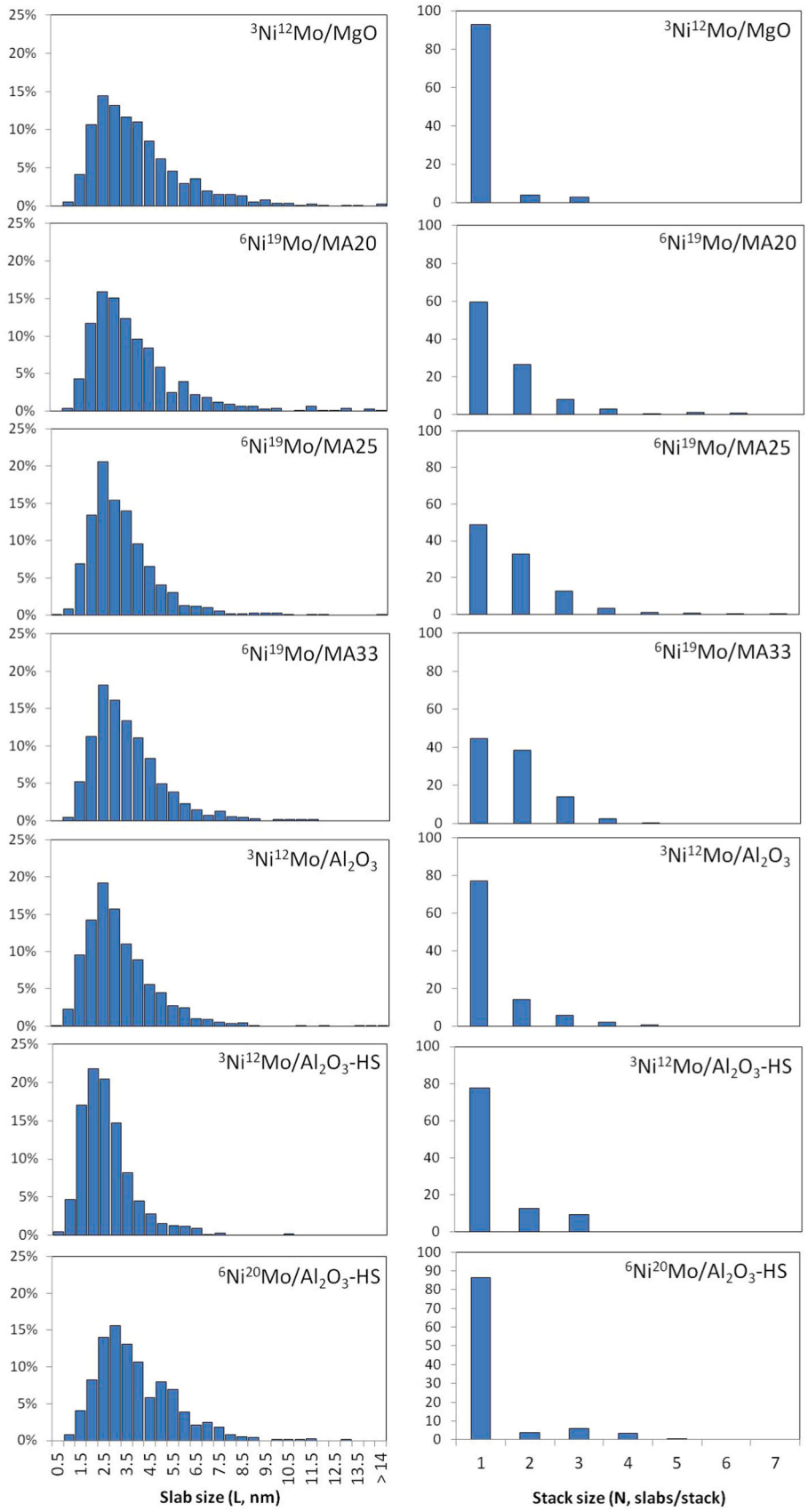

Fig. 2. (Ni)MoS_2 Slab and stack size distribution for the different NiMo-based catalysts.

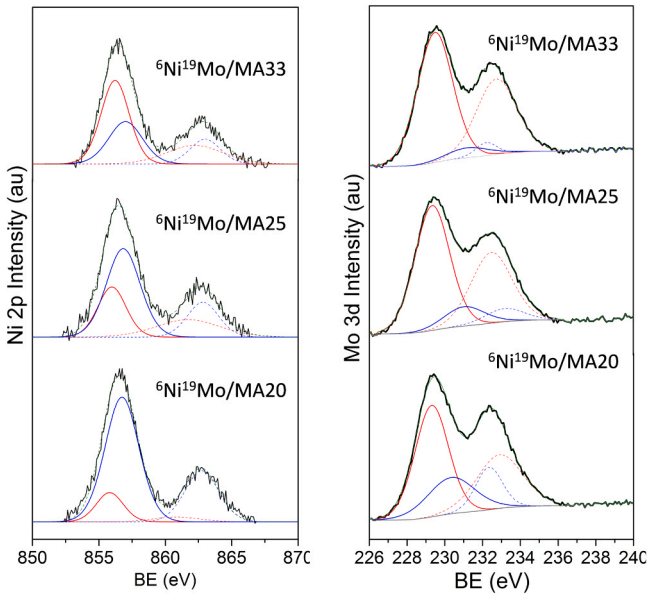

Fig. 3. XPS spectrum of the Ni $2p_{3/2}$ component (left side) and Mo $3d_{5/2}$ components (right side) for the MgAl-based catalyst with different Mg to Al ratio in their calcined form.

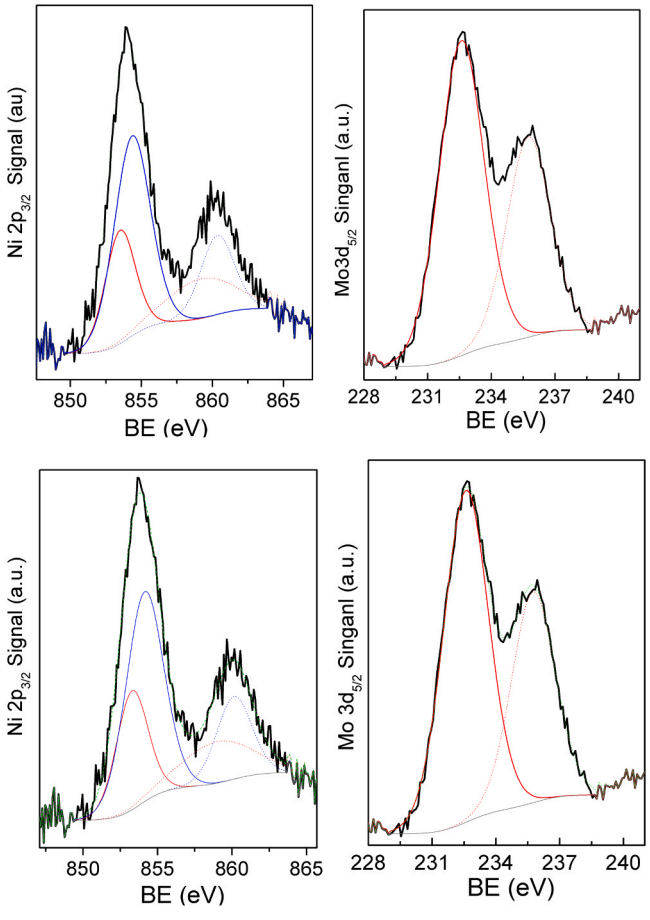

Fig. 4. XPS spectrum of the Ni 2p3/2 (left side) and Mo $3d_{5/2}$ (right side) components for the $^{3}Ni^{12}Mo/Al_2O_3$–HS (upper side, a, b) and $^{3}Ni^{12}Mo/MgO$ (lower side, c,d) catalysts in their calcined form.

Table 2
Binding energies of MgO-, LDH-, and Al_2O_3-based catalysts in their oxidic form.

Sample	Mo $3d_{5/2}$ BE (FWHM, %)		Ni $2p_{3/2}$ BE (FWHM, %)		
	MoOx	MoO_3	Ni^0	NiO/ $NiMoO_4$	$NiAl_2O_4$
$^{3}Ni^{12}Mo/MgO$	–	232.2 (2.2, 100%)	852.2 (3.0 37.9%)	855.3 (3.0, 62.1%)	–
$^{6}Ni^{19}Mo/MA20$	229.3 (2.2, 68.5%)	230.3 (2.4, 31.5%)	–	855.8 (2.5, 17.7%)	856.7 (3.0, 85.3%)
$^{6}Ni^{19}Mo/MA25$	229.3 (2.2, 84.9)	231.1 (2.4, 15.1%)	–	855.9 (2.5, 38.2%)	856.9 (3.0, 61.8%)
$^{6}Ni^{19}Mo/MA33$	229.5 (2.2, 91.8%)	232.2 (2.4, 8.2%)	–	856.2 (2.6, 60.8%)	857.0 (3.0, 39.2%)
$^{3}Ni^{12}Mo/Al_2O_3$-HS	–	232.6 (2.4, 100%)	–	856.7 (2.5, 88.9)	857.4 (3.0, 11.1%)

contribution of $NiAl_2O_4$ to the Ni $2p_{3/2}$ component increases with the Mg content. Thus, the XPS results suggest that the presence of Mg favors the reaction between Al and Ni to form $NiAl_2O_4$.

The shifting of BE values observed may indicate changes in the electronic density of the Ni and Mo oxide particles on the different NiMo catalysts. Yet, there can be other effects, as for instance, change in particle size and/or final relaxation effects, contributing to the observed BE values of the different components [54–56]. In order to identify the possible contribution of these final state effects and to evaluate properly the shifting of BE observed for this series of catalysts, the auger parameter (α) has been calculated. This parameter allows evaluating the particle charge (as compared to a reference sample) independently of final state effects.

The Ni auger parameter can be calculated as indicated in Eq. (1).

$$\alpha = BE\ (Ni) + KE(Ni) \quad (1)$$

where BE(Ni) is the binding energy of the Ni $2p_{3/2}$ electrons and KE(Ni) is the kinetic energy of the Ni Auger electrons. Combining the Auger parameter with the binding energy values obtained for a given specie, initial state contributions ($\Delta\varepsilon = \varepsilon_{sample} - \varepsilon_{reference}$) can be obtained by comparison with a reference sample, as indicated in Eq. (2).

$$\Delta\varepsilon = \Delta BE + (\Delta\alpha/2) \quad (2)$$

For these calculations, the Al_2O_3-based catalyst has been taken as reference sample. Thus, the charge of $NiO/NiMoO_4$ particles has been referred to the particle charge of catalyst $NiMo/Al_2O_3$, and the results obtained are included in Table 3.

As can be seen there, $NiO/NiMoO_4$ particles for all three LDH-and MgO-based catalysts present a negative charge as compared to those of the $NiMo/Al_2O_3$-HS catalyst. Within the LDH-catalyst series, the negative charge of the $NiO/NiMoO_4$ particles increases with the Mg content of the support of the catalyst or, in other words, with increasing the basicity of the support. Indeed, NiMo/MgO catalyst, holding the strongest basic sites according to the Knoevenagel reaction tests, shows the most negative particle charge value of this series of catalyst. This can

Table 3
Ni Auger parameter calculated for the Ni$2p_{3/2}$ component assigned to NiO/ $NiMoO_4$.

Sample	KE (Ni)	BE Ni (eV)	(eV)	(eV)
$^{3}Ni^{12}Mo/Al_2O_3$	833.98	860.4	1694.4	0 (ref)
$^{6}Ni^{19}Mo/MA33$	841.00	858.0	1699.0	-0.13
$^{6}Ni^{19}Mo/MA25$	841.07	858.0	1699.0	-0.15
$^{6}Ni^{19}Mo/MA20$	841.29	857.6	1698.9	-0.63
$^{3}Ni^{12}Mo/MgO$	833.70	860.0	1693.7	-0.77

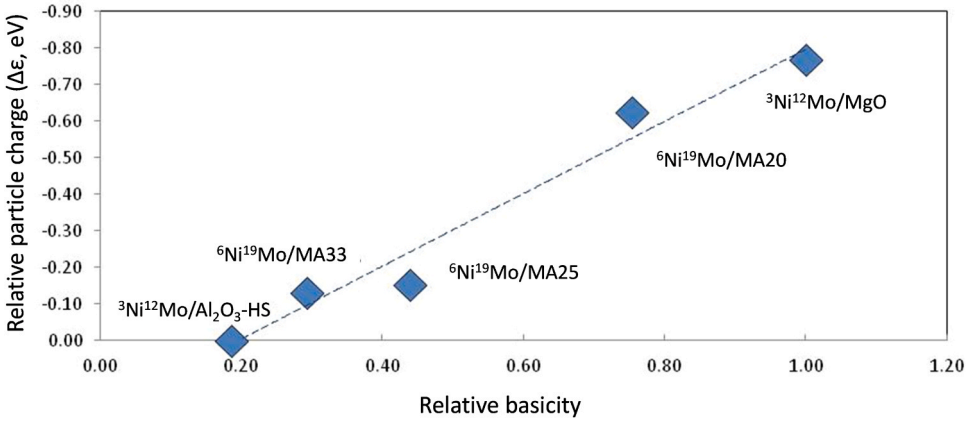

Fig. 5. Relative particle charge of $NiO/NiMoO_4$ (reference $NiMo/Al_2O_3$-HS catalyst) as function of the relative basicity (to MgO) of the support of the corresponding catalysts.

be clearly seen in Fig. 5 where the particle charge of $NiO/NiMoO_4$ (relative to $NiMo/Al_2O_3$) is plotted as a function of the basicity relative to MgO of each of the catalysts. Almost a linear correlation between both parameters is obtained. Despite the fact that Mo Auger cannot be properly measured, the shifting of the BE of Mo 3d towards lower values with increasing basicity of the corresponding support suggest a similar effect for MoO_3 supported particles.

3.2. Catalytic test: hydrogenation of 1-methylnaphthalene

The different catalysts of this series have been evaluated for the hydrogenation of a model feed containing 1-methylnaphthalene (1-MN) and dibenzothiophene (DBT) solved in normal heptane (see experimental). The activity test were carried out at 350 ºC, 30 bar pressure, G/L= 1000 Nm^3/m^3 as described in Section 2.4.

Fig. 6 shows the hydrogenation rates of 1-MN for the different catalysts. It can be seen that catalysts $^{6}Ni^{20}Mo/MA20$, $^{6}Ni^{20}Mo/Al_2O_3$-HS and $^{3}Ni^{12}Mo/Al_2O_3$-HS are the most active ones followed by $^{6}Ni^{20}Mo/MA25$, $^{3}Ni^{12}Mo/MgO$, $^{6}Ni^{20}Mo/MA33$ and $^{3}Ni^{12}Mo/Al_2O_3$. As mentioned in the introduction, differences in catalytic activity can be ascribed to different catalyst features such as metal loading, dispersion of the sulfided phase or effective mixing of the Ni and Mo phase. Therefore, in order to rule out the effect of metal loading and the dispersion of NiMo–S phase, the intrinsic activity for each catalyst has been estimated on the basis of the HR-TEM distribution and the metal loading of each catalyst.

(Ni)MoS_2 slabs are structure-sensitive and the different catalytic functions, namely hydrogenation (HYD) and hydrodesulfurization (HDS, DDS or HyDS) occur on different sites. As commonly agreed in the literature, the sites of particular importance for HYD and HDS (promoted or not) are located at edge positions while those of the basal plane are relatively inert [57–60]. Therefore, we have considered that only the Mo atoms located at the edge and corner positions (in single slabs) are active for the hydrogenation and desulfurization reactions. On the other hand, single MoS_2 slabs have been described employing different geometries as, for instance, chain-like, triangular, hexagonal or rhombohedric [61]. Topsøe and coworkers [62] showed, on an atom resolved scale, by high-resolution scanning tunneling microscopy (STM) in

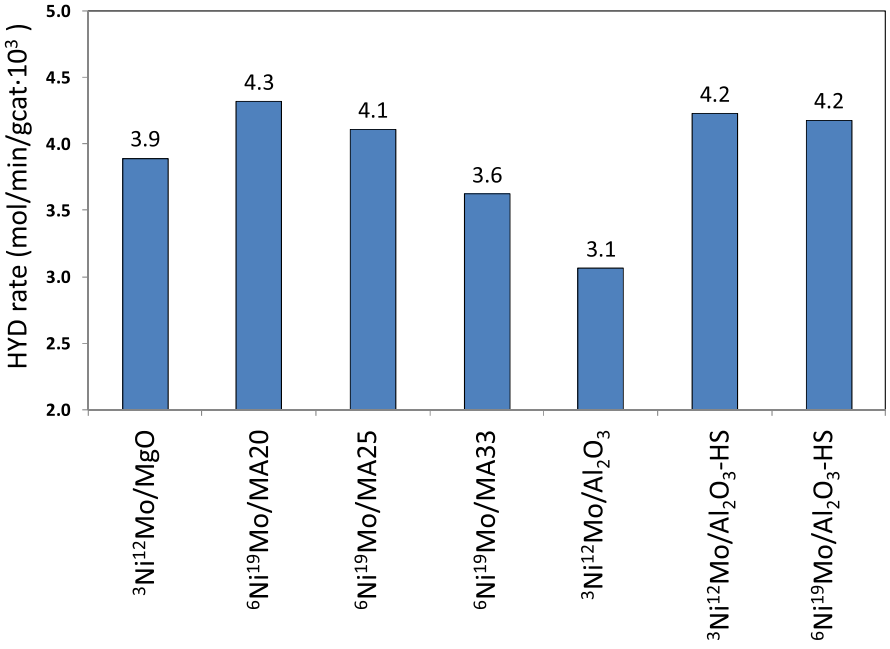

Fig. 6. 1-MN hydrogenation rate for the different NiMo catalysts at 350 ºC, 30 bar, G/L= 1000 and LHSV of 0.125 h^{-1}.

combination with density-functional theory (DFT), that NiMoS2 presents a hexagonal geometry.

Taking into account the above preliminary considerations, the amount of active (Ni)Mo atoms has been estimated from the following four hypothesis (see Scheme 2): 1) All the MoS_2 slabs present a hexagonal geometry. 2) In a single slab, only the Mo located at edge and corner positions are active for the hydrogenation or desulfurization reactions. Those contained in the basal plane of the slab do not catalyze any of the two reactions. 3) The hexagonal geometry is regular and therefore can be described by a geometrical model accordingly. Then, following the model of Kasztelan et al. [61], Mo atoms in a single hexagonal MoS_2 slab are mathematically described as described in Eqs. (3)–(5) (see Scheme 2). and 4) The Mo active sites for hydrogenation are located only in slabs holding MoS_2 basal planes in contact with the reactant molecules. Thus, in MoS_2 stacks, the amount of active sites has to be corrected according to the average number of slabs forming the stack (see Eqs. (6)–(8) and Scheme 1).

$$^{Basal}Mo = n_1^{\,2} + 2n_1.n_2 - 5n_1 - 3n_2 + 6 \quad n_1, n_2 > 2 \tag{3}$$

$$^{Edge}Mo = 3n_1 + 3n_2 - 12 \tag{4}$$

$$^{Corner}Mo = 6 \tag{5}$$

where n_1 and n_2 are the number of Mo ions in the different sides of a single slab [61].

$$L = \frac{\sum_i L_i}{n_T} \tag{6}$$

$$Stk = \frac{\sum_{i}^{Stack} L_i}{\sum_{i}^{Single\ \ slab} L_i} \tag{7}$$

$$N = \sum_i \frac{P_i}{100} \cdot N_i \tag{8}$$

where L is the length of a single slab and P_i is the percentage of stacks formed by i slabs.

On basis of the average $NiMoS_2$ slab size and stack distribution and the four working hypotheses, the amount of Mo atoms in RIM (^{RIM}Mo active for hydrogenating reactions) and edge positions (active for direct desulfurization) have been calculated for each of the catalyst (see Eqs. (9) and (10)). The results are included in Table 4.

$$\%RIM = \%RIM_{Single\ \ slabs} + \%RIM_{Stacks\ \ of\ \ i\ \ slabs} \tag{9}$$

$$\%Edge = (\%Edge + Corner)\cdot(100 - Stk) + (\%Edge + Corner)\cdot Stk/N \tag{10}$$

As can be seen, the catalysts with higher proportion of Mo atoms in RIM position are, in this order, the $NiMo/Al_2O_3$ and NiMo/MgO. Thus, despite the fact that the MoS_2 slabs are, on average basis, larger on NiMo/MgO as compared to the rest of catalysts, the low stacking degree compensates the high proportion of Mo atoms in MoS_2 basal planes by decreasing the Edge/RIM ratio far below that of the rest of catalysts of the series. The LDH-based catalysts present the lowest proportion of Mo atoms in RIM position due to the higher stacking degree and the relatively big slab particle size (around 3.5 nm).

Table 4
Results of the HR-TEM analysis of slab and stack size distribution and calculation of ^{RIM}Mo and ^{Edge}Mo for each catalyst.

Sample	Mo	HR-TEM results			Proportion of Mo active sites		mmol^{RIM}Mo / $g_{CAT}\cdot10^2$
	wt %	L (nm)	Stk (%)	N	% RIM	% Edge	
$^{3}Ni^{12}Mo$/MgO	12.7	3.7	7.1	2.0	8.2	0.1	8.2
$^{6}Ni^{19}Mo$/MA20	19.0	3.6	40.3	2.6	6.5	2.8	8.6
$^{6}Ni^{19}Mo$/MA25	19.0	3.4	51.2	2.3	6.7	2.8	8.8
$^{6}Ni^{19}Mo$/MA33	18.7	3.3	55.5	2.4	6.6	3.3	8.8
$^{3}Ni^{12}Mo$/Al_2O_3	12.0	3.0	22.8	2.5	11.8	1.9	10.2
$^{3}Ni^{12}Mo$/Al_2O_3-HS	12.2	2.4	10.4	2.3	13.4	0.7	14.6
$^{6}Ni^{20}Mo$/Al_2O_3-HS	20.0	3.6	13.7	3.7	7.9	0.7	11.0

Taking into account these calculations and the metal loading of each catalyst, the amount of Mo atoms in RIM positions per gram of catalyst has been calculated and included in Table 4. As can be seen, Al_2O_3-based catalyst with the optimal metal loadings presents the highest amount of hydrogenating sites (RIM Mo atoms per g of catalyst), even in spite of their lower loading as compared to the LDH-based catalyst. MgO- and LDH-based catalysts present a similar amount of hydrogenating sites per g of catalyst. According to the amount of ^{RIM}Mo per gram of catalyst, the intrinsic hydrogenation rate of each catalyst has been estimated and included in Fig. 7.

As can be seen, the intrinsic activity decreases in this order: NiMo/MgO > LDH-based catalyst (NiMo/MA20 > NiMo/MA25 > NiMo/MA33) > Al_2O_3–based catalysts. As previously reported by Kooyman et al. [13] one may consider that $NiMoS_2$ slab size or stacking degree may have an influence on their intrinsic hydrogenation activity. However, in this series of samples, there is no plausible correlation between the (Ni)MoS_2 slab size or stacking degree and hydrogenation activity. As can be seen in Fig. 7, samples with very different stacking degree ($^{3}Ni^{12}Mo$/MgO vs $^{6}Ni^{19}Mo$/MA20 catalysts) presents similar intrinsic hydrogenation rates and samples with similar (low) stacking degree (MgO vs Al_2O_3-HS based catalysts) present very different catalytic activity.

On the other hand, some samples suggest that the intrinsic hydrogenation rate decreases for smaller $NiMoS_2$ slab size ($^{3}Ni^{12}Mo$/MgO vs $^{6}Ni^{19}Mo$/MA33), while some others ($^{3}Ni^{12}Mo/Al_2O_3$ vs $^{3}Ni^{12}Mo/Al_2O_3$-HS) show the opposite trend on the HYD activity of the catalysts. Therefore, any possible effect derived from the $NiMoS_2$ slab size or

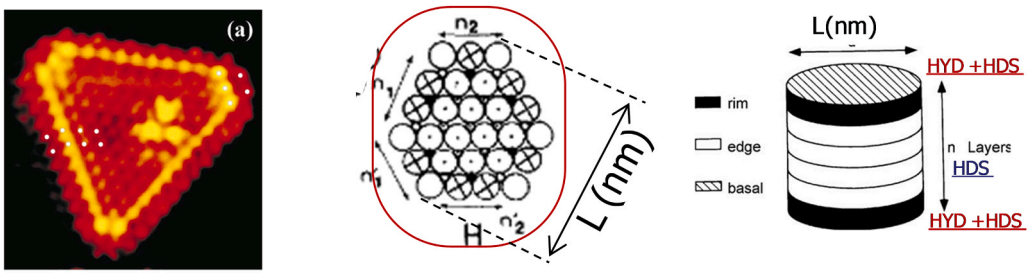

Scheme 2. Representation of the hypothesis assumed for the calculation of the amount of active sites in the sulfided catalyst. From left side to the right, morphology of a single slab (Ref. [18]), geometrical model (Ref. [61]) and MoS_2 stack model (Ref [63]).

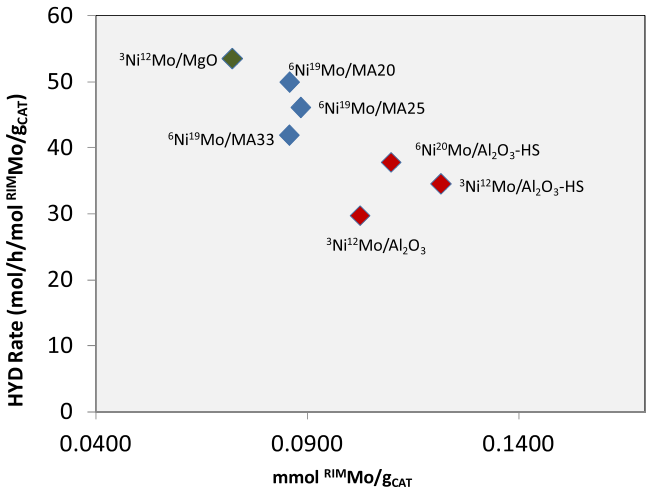

Fig. 7. Intrinsic 1-MN hydrogenation rate as function of the number of active sites for the different catalyst of this series.

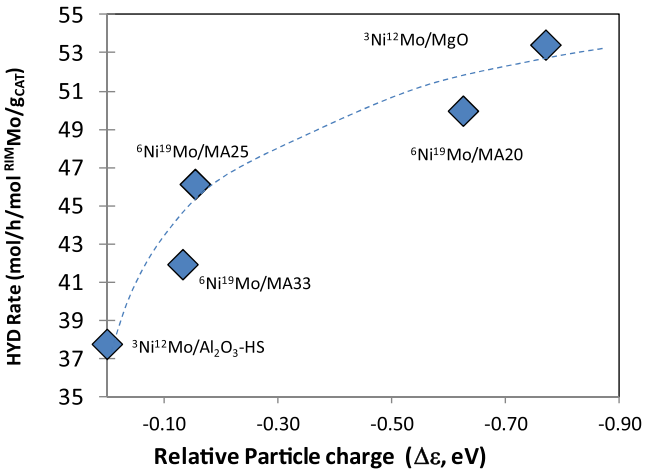

Fig. 9. Intrinsic hydrogenation rate of 1-MN as function of NiMo surface charge estimated by the XPS and Ni Auger measurements (relative to reference sample $^{3}Ni^{12}Mo/Al_2O_3$) for the different catalysts.

stacking degree can be ruled out, at least within the experimental ranges considered. It is then clear that the activity trends showed in Fig. 7 suggest that an alternative effect to slab size or stacking degree much exist. Thus, if we now plot the intrinsic hydrogenation rate of the NiMo–S phase versus basicity of the corresponding supports, a good correlation is obtained (Fig. 8). It appears then that the intrinsic hydrogenation rate increases when increasing the basicity of the support and levels off for the most basic MgO support.

As mentioned in the introduction, it is commonly accepted that the promotional effect of Ni (or Co) on Mo sulfides is due to an electron transfer phenomena from Ni to the Mo–S active sites in the sulfided slab [4,63–65]. Considering the fact that the basicity of the supports accounts also for their electrodonor capacity, the correlation found between hydrogenation activity and support basicity suggests that supports showing electrodonor capacity could induce a similar promoting effect than Ni or Co on the MoS_2 phase. Therefore, an enrichment of the electronic density of the MoS_2 slabs induced by basic (electrodonor) support could explain the correlation between intrinsic hydrogenation rate and basicity (Fig. 8).

According to these results, we postulate that strong basic sites on MgO and MgAl (LDH-derived) oxides may contribute to enriching the electronic density of the MoS_2 supported slabs. This may enhance the promoter effect of Ni or act itself as a MoS_2 promoter in a similar way as Ni or Co promoters do by means of an electron transfer phenomena. Thus, metal-S anti-bonding electrons from Ni would be moved to Mo-S antibonding orbitals, favoring the formation of vacancies on the MoS_2 where reactant molecules could be easily adsorbed and activated.

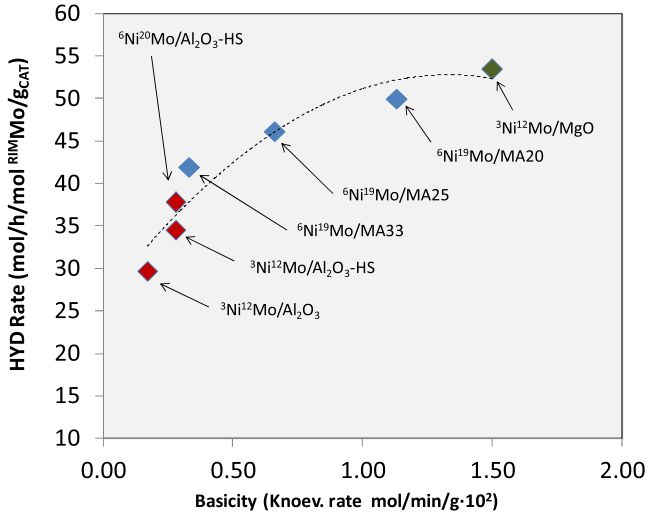

Fig. 8. Intrinsic hydrogenation rate as function of the basicity of the catalyst's support.

These results are consistent with the XPS characterization, the basicity of the support and the intrinsic hydrogenation rate measured for the different catalysts. Fig. 9 shows the good correlation found between the physico-chemical properties of the supports, the NiMo surface charge and their hydrogenation activity. As can be seen, there is a clear and positive correlation between the surface charge induced by the support on the NiMo oxide supported particles and the intrinsic hydrogenation rate of the corresponding $NiMoS_2$ slabs formed upon sulfidation of the formers.

The results presented in Fig. 9 are, therefore, a clear confirmation of the proposed charge transfer effect induced by the support to the NiMo-S supported slabs.

4. Conclusions

The physico-chemical characterization and catalytic activity of a series of catalyst supported on Al_2O_3, LDH-derived MgAl oxides and MgO have been investigated.

XPS measurements of calcined samples show a clear increase of the electron density of the supported particles (NiMo oxides) with the increasing basicity of the support. These results suggest an electron transfer phenomena to the $NiMoS_2$ slabs induced by the support, similar to that ascribed to the promoting effect of Ni or Co on MoS_2 active site.

On the other hand, the hydrogenation rate of 1-MN per active site has been obtained for each catalyst according to the RIM model and the NiMo–S phase dispersion (slab size and stacking degree) evaluated by a thorough HR-TEM study. The results obtained indicate that the intrinsic hydrogenation rate of the NiMo–S (supported) phase (irrespectively of the slab size or stacking degree) does not correlate with the slab size or stacking degree of the active NiMoS phase, but with the electron density of the supported particles, which is a function of the electrodonor capacity or basicity of the corresponding support (NiMo/MgO > NiMo/MgAl-LDHs > NiMo/Al_2O_3).

According to the physico-chemical characterization and the catalytic tests, it can be concluded that the enhancement of the hydrogenation activity of $NiMoS_2$ slabs supported on basic materials is due to an electronic enrichment induced by the support through an electron transfer phenomena that would favor the formation of S vacancies on the MoS_2 slab, where reactant molecules are adsorbed and activated.

The results presented here show a clear and specific support effect on the electronic properties of the supported NiMo oxides and on the catalytic properties of the supported NiMo–S phase. Thus, this contribution experimentally proves that the supports of TMs catalysts play a decisive role on the catalytic activity of the sulfided phase, which goes beyond the well known dispersing and stabilizing effects. In addition, it helps clarifying and understanding the, up to date, undefined "support effect" widely used in the literature during the last years to describe unexplained results.

CRediT authorship contribution statement

Carlos López-Cruz: Methodology, Validation, Investigation, Writing – original draft. **Javier Guzmán**: Investigation, Writing – review & editing, Supervision. **Guang Cao**: Writing – review & editing, Supervision. **Cristina Martínez**: Writing – original draft, Writing – review & editing, Supervision. **Avelino Corma**: Conceptualization, Writing – original draft, Writing – review & editing, Supervision, Project administration, Funding acquisition.

Declaration of Competing Interest

The authors declare that they have no known competing financial interests or personal relationships that could have appeared to influence the work reported in this paper.

Acknowledgements

This work has been supported by ExxonMobil Research and Engineering and by the Spanish Government through RTI2018-101033-B-I00 (MCIU/AEI/FEDER, UE). We thank the Electron Microscopy Service of the UPV for their help in sample characterization.

References

[1] R.N. Pease, W.B. Keighton, Removal of thiophene from benzene by catalytic hydrogenation Part I, Ind. Eng. Chem. 25 (1933) 1012–1013, https://doi.org/10.1021/ie50285a019.
[2] H. Beuther, R.A. Flinn, J.B. McKinley, For better hydrodesulfurization activity of promoted molybdenum oxide–alumina catalysts, Ind. Eng. Chem. 51 (1959) 1349–1350, https://doi.org/10.1021/ie50599a023.
[3] S. Harris, R.R. Chianelli, Catalysis by transition metal sulfides: the relation between calculated electronic trends and HDS activity (https://doi.org/), J. Catal. 86 (1984) 400–412, https://doi.org/10.1016/0021-9517(84)90385-3.
[4] S. Harris, R.R. Chianelli, Catalysis by transition metal sulfides: a theoretical and experimental study of the relation between the synergic systems and the binary transition metal sulfides (https://doi.org/), J. Catal. 98 (1986) 17–31, https://doi.org/10.1016/0021-9517(86)90292-7.
[5] A. Tan, S. Harris, Electronic structure of Rh2S3 and RuS2, two very active hydrodesulfurization catalysts, Inorg. Chem. 37 (1998) 2215–2222, https://doi.org/10.1021/ic971028n.
[6] M.J. Ledoux, O. Michaux, G. Agostini, P. Panissod, The influence of sulfide structures on the hydrodesulfurization activity of carbon-supported catalysts, J. Catal. 102 (1986) 275–288, https://doi.org/10.1016/0021-9517(86)90164-8.
[7] R.R. Chianelli, G. Berhault, P. Raybaud, S. Kasztelan, J. Hafner, H. Toulhoat, Periodic trends in hydrodesulfurization: in support of the Sabatier principle, Appl. Catal. A Gen. 227 (2002) 83–96, https://doi.org/10.1016/S0926-860X(01)00924-3.
[8] G.C.A. Schuit, B.C. Gates, Chemistry and engineering of catalytic hydrodesulfurization, AIChE J. 19 (1973) 417–438, https://doi.org/10.1002/aic.690190303.
[9] R.J.H. Voorhoeve, J.C.M. Stuiver, The mechanism of the hydrogenation of cyclohexene and benzene on nickel-tungsten sulfide catalysts, J. Catal. 23 (1971) 243–252, https://doi.org/10.1016/0021-9517(71)90046-7.
[10] A.L. Farragher, P. Cossee, No Title, in: J.W. Hightower (Ed.), 5th Int. Congr. Catal., Amsterdam, 1973: p. 1301.
[11] G. Hagenbach, P. Courty, B. Delmon, Physicochemical investigations and catalytic activity measurements on crystallized molydbenum sulfide-cobalt sulfide mixed catalysts, J. Catal. 31 (1973) 264–273, https://doi.org/10.1016/0021-9517(73)90333-3.
[12] M. Daage, R.R. Chianelli, Structure-function relations in molybdenum sulfide catalysts: the "Rim-Edge" model, J. Catal. 149 (1994) 414–427, https://doi.org/10.1006/jcat.1994.1308.
[13] E.J.M. Hensen, P.J. Kooyman, Y. van der Meer, A.M. van der Kraan, V.H.J. de Beer, J.A.R. van Veen, R.A. van Santen, The relation between morphology and hydrotreating activity for supported MoS2 particles, J. Catal. 199 (2001) 224–235, https://doi.org/10.1006/jcat.2000.3158.
[14] C. Liu, X.-Y. Cui, Y.-H. Song, M.-L. Zhu, Z.-T. Liu, Z.-W. Liu, The active nature of crystal MoS2 for converting sulfur-containing syngas, ChemCatChem 11 (2019) 1112–1122, https://doi.org/10.1002/cctc.201801588.
[15] W. Wang, L. Li, K. Wu, G. Zhu, S. Tan, W. Li, Y. Yang, Hydrothermal synthesis of bimodal mesoporous MoS2 nanosheets and their hydrodeoxygenation properties, RSC Adv. 5 (2015) 61799–61807, https://doi.org/10.1039/C5RA09690A.
[16] H. Topsøe, B.S. Clausen, R. Candia, C. Wivel, S. Mørup, In situ Mössbauer emission spectroscopy studies of unsupported and supported sulfided Co□Mo hydrodesulfurization catalysts: evidence for and nature of a Co□Mo□S phase, J. Catal. 68 (1981) 433–452, https://doi.org/10.1016/0021-9517(81)90114-7.
[17] R. Candia, B.S. Clausen, H. Topsøe, The origin of catalytic synergy in unsupported Co□Mo HDS catalysts, J. Catal. 77 (1982) 564–566, https://doi.org/10.1016/0021-9517(82)90199-3.
[18] I. Alstrup, I. Chorkendorff, R. Candia, B.S. Clausen, H. Topsøe, A combined X-ray photoelectron and Mössbauer emission spectroscopy study of the state of cobalt in sulfided, supported, and unsupported Co□Mo catalysts, J. Catal. 77 (1982) 397–409, https://doi.org/10.1016/0021-9517(82)90181-6.
[19] O. Sørensen, B.S. Clausen, R. Candia, H. Topsøe, Hrem and Aem studies of hds catalysts: direct evidence for the edge location of cobalt in Co–Mo–Sa, Appl. Catal. 13 (1985) 363–372, https://doi.org/10.1016/S0166-9834(00)81154-9.
[20] H. Topsøe, B.S. Clausen, Active sites and support effects in hydrodesulfurization catalysts, Appl. Catal. 25 (1986) 273–293, https://doi.org/10.1016/S0166-9834(00)81246-4.
[21] S. Helveg, J.V. Lauritsen, E. Lægsgaard, I. Stensgaard, J.K. Nørskov, B.S. Clausen, H. Topsøe, F. Besenbacher, Atomic-scale structure of single-layer MoS2 nanoclusters, Phys. Rev. Lett. 84 (2000) 951–954, https://doi.org/10.1103/PhysRevLett.84.951.
[22] J. Kibsgaard, B.S. Clausen, H. Topsøe, E. Lægsgaard, J.V. Lauritsen, F. Besenbacher, Scanning tunneling microscopy studies of TiO2-supported hydrotreating catalysts: anisotropic particle shapes by edge-specific MoS2–support bonding, J. Catal. 263 (2009) 98–103, https://doi.org/10.1016/j.jcat.2009.01.016.
[23] A.S. Walton, J.V. Lauritsen, H. Topsøe, F. Besenbacher, MoS2 nanoparticle morphologies in hydrodesulfurization catalysis studied by scanning tunneling microscopy, J. Catal. 308 (2013) 306–318, https://doi.org/10.1016/j.jcat.2013.08.017.
[24] S. Eijsbouts, On the flexibility of the active phase in hydrotreating catalysts, Appl. Catal. A Gen. 158 (1997) 53–92, https://doi.org/10.1016/S0926-860X(97)00035-5.
[25] X. Liu, Q. Wei, W. Huang, Y. Zhou, P. Zhang, Z. Xu, DFT insights into the stacking effects on HDS of 4,6-DMDBT on Ni–Mo–S corner sites, Fuel 280 (2020), 118669, https://doi.org/10.1016/j.fuel.2020.118669.
[26] S. Eijsbouts, L.C.A. van den Oetelaar, R.R. van Puijenbroek, MoS2 morphology and promoter segregation in commercial Type 2 Ni–Mo/Al2O3 and Co–Mo/Al2O3 hydroprocessing catalysts (https://doi.org/), J. Catal. 229 (2005) 352–364, https://doi.org/10.1016/j.jcat.2004.11.011.
[27] M.S. Rana, S.K. Maity, J. Ancheyta, G. Murali Dhar, T.S.R. Prasada Rao, MoCo(Ni)/ZrO2–SiO2 hydrotreating catalysts: physico-chemical characterization and activities studies, Appl. Catal. A Gen. 268 (2004) 89–97, https://doi.org/10.1016/j.apcata.2004.03.023.
[28] C. Leyva, M.S. Rana, J. Ancheyta, Surface characterization of Al2O3–SiO2 supported NiMo catalysts: an effect of support composition, Catal. Today 130 (2008) 345–353, https://doi.org/10.1016/j.cattod.2007.10.113.
[29] B. Demirel, W.H. Wiser, High conversion (98%) for the hydrogenation of 1-methylnaphthalene to methyldecalins, Fuel Process. Technol. 53 (1997) 157–169, https://doi.org/10.1016/S0378-3820(97)00044-1.
[30] D. Zhang, A. Duan, Z. Zhao, G. Wan, Z. Gao, G. Jiang, K. Chi, K.H. Chuang, Preparation, characterization and hydrotreating performances of ZrO2–Al2O3-supported NiMo catalysts, Catal. Today 149 (2010) 62–68, https://doi.org/10.1016/j.cattod.2009.04.012.
[31] R. Cattaneo, T. Shido, R. Prins, A. XANES, temperature-programmed sulphidation study of modified NiMo/SiO2 hydrotreating catalysts, in: B. Delmon, G.F. Froment, P.B.T.-S. in S.S., C. Grange (Eds.), Hydrotreatment Hydrocracking Oil Fractions, Elsevier, 1999, pp. 421–425, https://doi.org/10.1016/S0167-2991(99)80444-3.
[32] S.M.A.M. Bouwens, R. Prins, V.H.J. De Beer, D.C. Koningsberger, Structure of the molybdenum sulfide phase in carbon-supported molybdenum and cobalt-molybdenum sulfide catalysts as studied by EXAFS, J. Phys. Chem. 94 (1990) 3711–3718, https://doi.org/10.1021/j100372a065.
[33] J.A.R. van Veen, E. Gerkema, A.M. van der Kraan, A. Knoester, A real support effect on the activity of fully sulphided CoMoS for the hydrodesulphurization of thiophene, J. Chem. Soc. Chem. Commun. (1987) 1684–1686, https://doi.org/10.1039/C39870001684.
[34] J. Cinibulk, P.J. Kooyman, Z. Vit, M. Zdražil, Magnesia-supported Mo, CoMo and NiMo sulfide catalysts prepared by nonaqueous impregnation: parallel HDS/HDN of thiophene and pyridine and TEM microstructure, Catal. Lett. 89 (2003) 147–152, https://doi.org/10.1023/A:1024748232539.
[35] M. Zdražil, MgO-supported Mo, CoMo and NiMo sulfide hydrotreating catalysts, Catal. Today 86 (2003) 151–171, https://doi.org/10.1016/S0920-5861(03)00409-7.
[36] L. Kaluza, J. Karban, D. Gulkova, Activity and selectivity of Co(Ni)Mo sulfides supported on MgO, Al2O3, ZrO2, TiO2, MCM-41 and activated carbon in parallel hydrodeoxygenation of octanoic acid and hydrodesulfurization of 1-benzothiophene, React. Kinet. Mech. Catal. 127 (2019) 887–902, https://doi.org/10.1007/s11144-019-01620-x.

[37] L. Zhang, W. Fu, M. Xiang, W. Wang, M. He, T. Tang, MgO nanosheet assemblies supported CoMo catalyst with high activity in hydrodesulfurization of dibenzothiophene, Ind. Eng. Chem. Res. 54 (2015) 5580–5588, https://doi.org/10.1021/acs.iecr.5b00452.
[38] Y. Kanda, K. Nakata, C. Temma, M. Sugioka, Y. Uemichi, Effects of support on formation of active sites and hydrodesulfurization activity of rhodium phosphide catalyst, J. Jpn. Pet. Inst. 55 (2012) 108–119, https://doi.org/10.1627/jpi.55.108.
[39] F. Cesano, S. Bertarione, A. Piovano, G. Agostini, M.M. Rahman, E. Groppo, F. Bonino, D. Scarano, C. Lamberti, S. Bordiga, L. Montanari, L. Bonoldi, R. Millini, A. Zecchina, Model oxide supported MoS2 HDS catalysts: structure and surface properties, Catal. Sci. Technol. 1 (2011) 123–136, https://doi.org/10.1039/c0cy00050g.
[40] T. Klimova, D. Solís Casados, J. Ramírez, New selective Mo and NiMo HDS catalysts supported on Al2O3–MgO(x) mixed oxides, Catal. Today 43 (1998) 135–146, https://doi.org/10.1016/S0920-5861(98)00142-4.
[41] F. Trejo, M.S. Rana, J. Ancheyta, CoMo/MgO–Al2O3 supported catalysts: an alternative approach to prepare HDS catalysts, Catal. Today 130 (2008) 327–336, https://doi.org/10.1016/j.cattod.2007.10.105.
[42] A. Guevara-Lara, A.E. Cruz-Pérez, Z. Contreras-Valdez, J. Mogica-Betancourt, A. Alvarez-Hernández, M. Vrinat, Effect of Ni promoter in the oxide precursors of MoS2/MgO–Al2O3 catalysts tested in dibenzothiophene hydrodesulphurization, Catal. Today 149 (2010) 288–294, https://doi.org/10.1016/j.cattod.2009.09.014.
[43] L. Wu, D. Jiao, J. Wang, L. Chen, F. Cao, The role of MgO in the formation of surface active phases of CoMo/Al2O3–MgO catalysts for hydrodesulfurization of dibenzothiophene, Catal. Commun. 11 (2009) 302–305, https://doi.org/10.1016/j.catcom.2009.10.021.
[44] T. Klicpera, M. Zdražil, Preparation of high-activity MgO-supported Co–Mo and Ni–Mo sulfide hydrodesulfurization catalysts (https://doi.org/), J. Catal. 206 (2002) 314–320, https://doi.org/10.1006/jcat.2001.3488.
[45] M.J. Climent, A. Corma, S. Iborra, K. Epping, A. Velty, Increasing the basicity and catalytic activity of hydrotalcites by different synthesis procedures, J. Catal. 225 (2004) 316–326, https://doi.org/10.1016/j.jcat.2004.04.027.
[46] F. Delannay, High resolution electron microscopy of hydrodesulfurization catalysts: a review, Appl. Catal. 16 (1985) 135–152, https://doi.org/10.1016/S0166-9834(00)84467-X.
[47] P.J. Kooyman, J.A.R. van Veen, The detrimental effect of exposure to air on supported MoS2, Catal. Today 130 (2008) 135–138.
[48] R.M. Martin-Aranda, M.F. Portela, L.M. Madeira, F. Freire, M. Oliveira, Effect of alkali metal promoters on nickel molybdate catalysts and its relevance to the selective oxidation of butane, Appl. Catal. A Gen. 127 (1995) 201–217, https://doi.org/10.1016/0926-860X(95)00037-2.
[49] R. Hernández-Huesca, J. Mérida-Robles, P. Maireles-Torres, E. Rodríguez-Castellón, A. Jiménez-López, Hydrogenation and ring-opening of tetralin on Ni and NiMo supported on alumina-pillared α-zirconium phosphate catalysts. A thiotolerance study, J. Catal. 203 (2001) 122–132, https://doi.org/10.1006/jcat.2001.3321.
[50] P. Dufresne, E. Payen, J. Grimblot, J.P. Bonnelle, Study of nickel-molybdenum-.gamma.-aluminum oxide catalysts by x-ray photoelectron and Raman spectroscopy. Comparison with cobalt-molybdenum-.gamma.-aluminum oxide catalysts, J. Phys. Chem. 85 (1981) 2344–2351, https://doi.org/10.1021/j150616a010.
[51] S. Kasztelan, J. Grimblot, J.P. Bonnelle, E. Payen, H. Toulhoat, Y. Jacquin, Preparation of Co–Mo-γAl2O3 and Ni–Mo-γAl2O3 catalysts by ph regulation of molybdenum solution. characterization of supported species and hydrogenation activities, Appl. Catal. 7 (1983) 91–112, https://doi.org/10.1016/0166-9834(83)80241-3.
[52] M. Shimoda, T. Hirata, K. Yagisawa, M. Okochi, A. Yoshikawa, Deconvolution of Mo 3d X-ray photoemission spectraγ-Mo4O11: agreement with prediction from bond length-bond strength relationships, J. Mater. Sci. Lett. 8 (1989) 1089–1091, https://doi.org/10.1007/BF01730497.
[53] M. Anwar, C.A. Hogarth, R. Bulpett, Effect of substrate temperature and film thickness on the surface structure of some thin amorphous films of MoO3 studied by X-ray photoelectron spectroscopy (ESCA), J. Mater. Sci. 24 (1989) 3087–3090, https://doi.org/10.1007/BF01139023.
[54] A. Zwijnenburg, A. Goossens, W.G. Sloof, M.W.J. Crajé, A.M. van der Kraan, L. Jos de Jongh, M. Makkee, J.A. Moulijn, XPS, Mössbauer, Characterization of Au/TiO2 propene epoxidation catalysts, J. Phys. Chem. B 106 (2002) 9853–9862, https://doi.org/10.1021/jp014723w.
[55] C.C. Chusuei, X. Lai, K. Luo, D.W. Goodman, Modeling heterogeneous catalysts: metal clusters on planar oxide supports, Top. Catal. 14 (2000) 71–83, https://doi.org/10.1023/A:1009059100646.
[56] S. Zafeiratos, S. Kennou, A study of gold ultrathin film growth on yttria-stabilized ZrO2(100), Surf. Sci. 443 (1999) 238–244, https://doi.org/10.1016/S0039-6028(99)01014-6.
[57] S.P. Kelty, A.F. Ruppert, R.R. Chianelli, J. Ren, M.-H. Whangbo, Scanning probe microscopy study of layered dichalcogenide ReS2, J. Am. Chem. Soc. 116 (1994) 7857–7863, https://doi.org/10.1021/ja00096a048.
[58] M. Salmeron, G.A. Somorjai, A. Wold, R. Chianelli, K.S. Liang, The adsorption and binding of thiophene, butene and H2S on the basal plane of MoS2 single crystals (https://doi.org/), Chem. Phys. Lett. 90 (1982) 105–107, https://doi.org/10.1016/0009-2614(82)83620-8.
[59] K.-I. Tanaka, in: D.D. Eley, H. Pines, P.B.B.T.-A. in, C. Weisz (Eds.), Catalysis Controlled by the Constitution of Active Sites, Academic Press, 1985, pp. 99–158, https://doi.org/10.1016/S0360-0564(08)60259-X.
[60] X. Liu, S. Ding, Q. Wei, Y. Zhou, P. Zhang, Z. Xu, DFT insights in to the hydrodenitrogenation behavior differences between indole and quinoline, Fuel 285 (2021), 119039, https://doi.org/10.1016/j.fuel.2020.119039.
[61] S. Kasztelan, H. Toulhoat, J. Grimblot, J.P. Bonnelle, A geometrical model of the active phase of hydrotreating catalysts, Appl. Catal. 13 (1984) 127–159, https://doi.org/10.1016/S0166-9834(00)83333-3.
[62] J.V. Lauritsen, S. Helveg, E. Lægsgaard, I. Stensgaard, B.S. Clausen, H. Topsøe, F. Besenbacher, Atomic-scale structure of Co–Mo–S nanoclusters in hydrotreating catalysts, J. Catal. 197 (2001) 1–5, https://doi.org/10.1006/jcat.2000.3088.
[63] A. Galtayries, J. Grimblot, Formation and electronic properties of oxide and sulphide films of Co, Ni and Mo studied by XPS, J. Electron Spectros. Relat. Phenom. 98–99 (1999) 267–275, https://doi.org/10.1016/S0368-2048(98)00292-8.
[64] F. Maugé, J.C. Duchet, J.C. Lavalley, S. Houssenbay, E. Payen, J. Grimblot, S. Kasztelan, The sulphided state of nickel molybdenum catalysts supported on zirconia and aluminates, Catal. Today 10 (1991) 561–577, https://doi.org/10.1016/0920-5861(91)80039-C.
[65] F.-S. Xiao, Q. Xin, X.-X. Guo, Catalytic activity of ruthenium promoted Co–Mo/Al2O3 and infrared investigation of carbon monoxide and nitric oxide adsorption, Appl. Catal. A Gen. 95 (1993) 21–34, https://doi.org/10.1016/0926-860X(93)80194-U.